Thermal infrared spectroscopy and modeling of experimentally shocked plagioclase feldspars

JEFFREY R. JOHNSON,[1,]* FRIEDRICH HÖRZ,[2] AND MATTHEW I. STAID[1]

[1]United States Geological Survey, 2255 N. Gemini Drive, Flagstaff, Arizona 86001, U.S.A.
[2]Johnson Space Center, SN-2, NASA, Houston, Texas 77058 U.S.A.

ABSTRACT

Thermal infrared emission and reflectance spectra (250–1400 cm^{-1}; ~7–40 μm) of experimentally shocked albite- and anorthite-rich rocks (17–56 GPa) demonstrate that plagioclase feldspars exhibit characteristic degradations in spectral features with increasing pressure. New measurements of albite (Ab$_{98}$) presented here display major spectral absorptions between 1000–1250 cm^{-1} (8–10 μm) (due to Si-O antisymmetric stretch motions of the silica tetrahedra) and weaker absorptions between 350–700 cm^{-1} (14–29 μm) (due to Si-O-Si octahedral bending vibrations). Many of these features persist to higher pressures compared to similar features in measurements of shocked anorthite, consistent with previous thermal infrared absorption studies of shocked feldspars. A transparency feature at 855 cm^{-1} (11.7 μm) observed in powdered albite spectra also degrades with increasing pressure, similar to the 830 cm^{-1} (12.0 μm) transparency feature in spectra of powders of shocked anorthite. Linear deconvolution models demonstrate that combinations of common mineral and glass spectra can replicate the spectra of shocked anorthite relatively well until shock pressures of 20–25 GPa, above which model errors increase substantially, coincident with the onset of diaplectic glass formation. Albite deconvolutions exhibit higher errors overall but do not change significantly with pressure, likely because certain clay minerals selected by the model exhibit absorption features similar to those in highly shocked albite. The implication for deconvolution of thermal infrared spectra of planetary surfaces (or laboratory spectra of samples) is that the use of highly shocked anorthite spectra in end-member libraries could be helpful in identifying highly shocked calcic plagioclase feldspars.

INTRODUCTION

The structural behavior of plagioclase feldspars under high static pressures is typically studied using thermal infrared absorption spectroscopy to better constrain the processes by which planetary interiors and crusts evolve over time (e.g., Williams and Jeanloz 1988, 1989; Daniel et al. 1997; Williams 1998). Complementary thermal infrared analyses of experimentally and naturally shocked feldspars serve to better understand shock-induced structural disorder by documenting changes in the position and strength of spectral absorptions as a function of shock pressure (e.g., Stöffler 1971; Stöffler and Hornemann 1972; Arndt et al. 1982; Ostertag 1983). This information is useful when interpreting surface mineralogy and/or physical properties from remotely sensed thermal infrared observations of the terrestrial planets and asteroids (e.g., Christensen et al. 1998, 2001; Sprague et al. 2002; Salisbury et al. 1995, 1997; Morris et al. 1999; Ramsey 2002) or in laboratory studies of shocked meteorites or impact crater materials (e.g., Cooney et al. 1999; Xie et al. 2001).

Johnson et al. (2002a) acquired thermal infrared (250–1400 cm^{-1}; ~7–40 μm) spectra of experimentally shocked anorthite samples over peak pressures from 17 to 56 GPa. They documented changes in the appearance and position of spectral bands with increasing pressure due to depolymerization of the sili-

cate tetrahedra, including strong absorption bands at 1115 cm^{-1} and near 940 cm^{-1}, weak bands in the 500–650 cm^{-1} region, and a transparency feature near 830 cm^{-1} in spectra of shocked powders. In this paper, we present similar spectra of experimentally shocked albite and compare the effects of shock on thermal infrared emission and reflectance spectra of plagioclase feldspars. We also use combinatorial spectral deconvolution techniques to investigate the degree to which combinations of other minerals can replicate the spectra of shocked feldspars, and the implications for analysis of remote sensing observations.

BACKGROUND

Early studies of thermal infrared absorption spectra of naturally shocked feldspars demonstrated a decrease in the spectral detail and intensity of absorption features with increasing pressure (Lyon 1963; Bunch et al. 1967, 1968). This degradation was attributable to lattice disordering and increasing glass content, particularly at shock pressures above ~20 GPa (Stöffler 1972, 1974; Stöffler and Hornemann 1972; Arndt et al. 1982; Ostertag 1983). Modest disordering of feldspar generally begins at pressures above 15–20 GPa, whereas maskelynite (diaplectic glass) forms in feldspars between ~30–45 GPa. Significant melting occurs above ~45 GPa (Stöffler 1972; Gibbons et al. 1975; Hörz and Cintala 1997; Velde et al. 1987, 1989), although the absolute strain rate, initial temperature, and shock pulse duration probably influence the precise shock stress for melting (Stöffler 2001; DeCarli et al. 2002; Fritz et al. 2002).

* E-mail: jrjohnson@usgs.gov

Within this pressure regime, the characteristic, fourfold (tetrahedral), strong coordination bonds of Si and Al in feldspars distort to weaker, less-polymerized bonds that approach sixfold (octahedral) coordination. The structural disorder results in the mutual existence of diaplectic glasses and crystalline phases throughout this pressure region, which provide characteristic vibrational frequencies in the thermal infrared.

Between 400 and 550 cm^{-1}, bending vibrations in the Si-O-Al planar ring structures in tectosilicates and diaplectic glasses occur. SiO_6 octahedral-stretching vibrations occur between 750 and 850 cm^{-1}, whereas Si-O-Si octahedral-bending vibrations cause several weaker absorptions between about 700 and 450 cm^{-1}. Absorptions in the 900–1200 cm^{-1} region are due to Si-O antisymmetric stretch motions of the silicate tetrahedral units in the structure (Bunch et al. 1967; Iiishi et al. 1971; Stöffler and Hornemann 1972; Arndt et al. 1982; Velde et al. 1987; Williams and Jeanloz 1988, 1989; Daniel et al. 1995, 1997; Williams 1998).

Although spectral differences in unshocked feldspars of varying compositions are well documented (e.g., Iiishi et al. 1971; Nash and Salisbury 1991), Ostertag (1983) showed that changes in the stretching and bending modes associated with Si-O, Si-O-Si, and Si-O-Al bonds in thermal infrared absorption spectra of experimentally shocked feldspars follow similar patterns with increasing pressure. Nonetheless, the precise peak shock pressures at which structural disorder and melting occur appear to vary among feldspar compositions, with conversion to diaplectic glass occurring at lower pressures for Ca-rich plagioclase than for Na-rich plagioclase and K feldspars (e.g., Ostertag 1983; Stöffler 1984; Williams and Jeanloz 1989; Williams 1998). As shown below, comparison of thermal infrared spectra of anorthite from Johnson et al. (2002a) to the albite spectra presented here are consistent with these previous studies.

METHODS

Shock recovery experiments

The shock experiments were performed with the Flat Plate Accelerator at the Johnson Space Center, Houston. This powder propellant gun launches flat metal plates for the production of planar shock waves in targets (cf., Gibbons et al. 1975). Details of the shock experiments can be found in Johnson et al. (2002a). Briefly, the geologic target was a disc cored from the rock sample, 12 mm in diameter and 1 mm thick. The disc was encapsulated into a metal holder and placed into a vacuum chamber where it was impacted by a metal flyer plate of some measured velocity. Following an experiment, a lathe was used to remove excess metal from the holder until the silicate target could be pried from its original target well. Careful prying allowed for the recovery of relatively large chips (2–10 mm) that were separated from the more fine-grained materials. The latter were powdered to a more homogeneous grain size (<20–30 μm). Unshocked samples also were powdered similarly and broken into smaller chips for better comparison to the shocked samples. Use of the 25 mm barrel allowed for recovery of up to 400 mg. Table 1 lists the details of each experiment.

Although the small target-discs could readily be manufactured from single-crystal feldspars, we instead used a polycrystalline and essentially monomineralic sample to avoid possible bias of crystal-lattice orientation relative to the propagating shock wave on the type and degree of shock deformation. This constraint required a target rock with millimeter-sized crystals of random orientations. One sample that fit these criteria was a low-temperature albitite acquired from the veins of a serpentine massif in Szklary Lower Silesia, Poland. This rock contains 97% albite (Ab$_{98}$), with minor amounts of quartz, K feldspar, amphibole, and sericite, all with grain sizes <1 mm (Muszynski and Natkaniec-Nowak 1992). The Fe contents of this sample are very low (400–1000 ppm) (Delaney et al. 2003). The density of the sample was determined to be ~2.60 g/cm^3, matching the density of pure albite (2.61 g/cm^3).

Therkelsen (2002) described the thin section optical properties of the shocked anorthosite samples of Johnson et al. (2002a). Undulous extinction and planar deformation features are present at pressures below 25 GPa. Nearly complete undulous extinction and mosaicism is observed in the 29 GPa sample along with the formation of maskelynite in small patches. By 38 GPa, only small regions of undulous extinction occur, with the remainder nearly completely transformed to diaplectic glass, and by 50.0 GPa, the samples are completely isotropic with complete transformation to diaplectic glass.

Delaney et al. (2003) studied the changes in Fe oxidation state of the shocked albite samples, but did not report optical properties. It is likely that similar changes in optical properties are present in the shocked albite samples, albeit with variations in the precise pressure ranges over which the transformation from mosaicism to diaplectic glass and complete isotropy occur, as described below.

Thermal infrared spectroscopy

Infrared spectrometers at the University of Hawaii (UH) and Arizona State University (ASU) were used to obtain directional hemispherical reflectance and emissivity spectra of the larger chips and powders. Acquisition of spectra using both UH and ASU instruments allowed comparison of reflectance and emission techniques and provide checks on the reproducibility of the results (cf., Mustard and Hays 1997; Johnson et al. 2002a). The UH operates a Nicolet 740 spectrometer capable of providing directional hemispherical reflectance (715–3300 cm^{-1}; 3–14 μm) [similar to the arrangement of Salisbury et al. (1991a, 1991b, 1994)] in which the external port of the spectrometer is fitted with an integrating sphere, coated inside with a diffusely reflecting gold surface, and a liquid nitrogen-cooled Hg-Cd-Te (MCT) detector (Johnson et al. 1998). The spectrometer was configured to provide 8 cm^{-1} resolution with 1000 scans co-added per sample spectrum, which was divided by the spectrum of a diffusely reflecting gold plate to provide a hemispherical reflectance spectrum. Unfortunately, all but the unshocked samples were insufficient in size to fully cover the infrared field of view of the spectrometer. To compensate for the small sample area, we placed the samples on cups that were plated with the same reflective gold surface as the interior of the integrating sphere and that were sufficiently large to fill the sample port. This arrangement provided consistent measurements for a sample's spectral reflectance but at the expense of uncertainties in the absolute reflectance values because a portion of the "sample" viewed by the spectrometer was the highly reflective, gold-plated sample cup. However, measurements of the larger unshocked samples that filled the sample port provided a baseline from which the shocked sample reflectance values could be scaled, and emissivity measurements of the same samples provided an additional check on the reflectance levels.

ASU operates a Nicolet Nexus 670 spectrometer equipped with an uncooled, deuterated triglycine sulfate (DTGS) detector adapted for emission spectroscopy (Ruff et al. 1997). Energy from a heated particulate sample (maintained at 80 °C) is collected by a parabolic mirror and directed toward the interferometer, and blackbodies at 70 °C and 100 °C are used for radiometric calibration. For this instrument, the infrared beam was confined to the sample by adjusting the sample location within the optical path. The spectrometer was configured to provide 4 cm^{-1} resolution with 180 scans co-added per spectrum.

TABLE 1. Detailed experimental conditions for the albitite shock recovery experiments

EIL no.*	Impact velocity (km/s)	Flyer plate†	Assembly	Peak pressure (GPa)
3315	1.340	Al2024	SS304	17.0
3313	1.130	SS304	SS304	24.0
3311	1.180	SS304	SS304	25.5
3322	1.271	SS304	SS304	27.8
3312	1.320	SS304	SS304	29.0
3314	1.410	SS304	SS304	31.4
3319	1.227	FS77	SS304	34.8
3318	1.320	FS77	FS77	38.0
3320	1.139	FS77	FS77	44.6
3316	1.250	FS77	FS77	50.0
3317	1.370	FS77	FS77	55.8

* EIL No. [Running Flat Plate Accelerator experiment number in Experimental Impact Laboratory (EIL) at Johnson Space Center].
† Projectile and assembly materials (Equation of State): Aluminum2024 (Marsh 1980), Stainless Steel 304 (Marsh 1980), "Fansteel 77" (a W-Ni alloy; Jones et al. 1966), W= pure tungsten (Marsh 1980).

Spectral deconvolutions

Deconvolution of remotely sensed spectra using libraries that include spectra of experimentally shocked feldspars potentially can help identify shocked materials on planetary surfaces (e.g., Johnson et al. 2002b). One important consideration when using these spectra, however, is whether combinations of other glass and unshocked mineral spectra could replicate their spectral features, thereby causing misidentification of shocked feldspars. To test this possibility, we used a combinatorial linear deconvolution model based on the multiple end-member spectral mixing algorithm (MESMA) of Roberts et al. (1998) to deconvolve the shocked feldspar emission spectra. In this technique, a given spectrum is modeled by a linear combination of specific end-members (e.g., Thompson and Salisbury 1993; Ramsey 2002; Bandfield 2002). For our end-member spectral library, we selected 32 common minerals from the ASU database (Christensen et al. 2000b), two K-rich and Si-rich glasses from Wyatt et al. (2001) and Hamilton et al. (2001), and the unshocked albitite and anorthosite spectra (Table 2). The combinatorial deconvolution algorithm selects the best subset of components required to model the input spectrum through iterative comparisons to the spectral library in order to minimize uncertainties in the derived fractional abundances.

The algorithm initially compared all possible six-end-member combinations based on the spectral library components and a blackbody (Staid et al. 2001). The blackbody was used to compensate for grain-size variations between the library spectra and the feldspar spectra. The best model containing positive end-member abundances for each input spectrum was identified on the basis of the root-mean-square (rms) error computed for each six-end-member combination. Then, each unused library end-member was alternately added to the six end-members and a new rms error was calculated. The spectrum that provided the best improvement (and was selected with a positive abundance for all end-member components) was then kept as a seventh end-member. If no additional spectrum resulted in all positive fractions and an improved error, six end-members comprised the solution. This procedure was then repeated until as many as nine end-members were selected. The algorithm produced fractions for each member chosen from the spectral library and a blackbody component. We ran the combinatorial demixing algorithm over the spectral range 400 to 1400 cm^{-1} with spectra of the shocked anorthosite chips from Johnson et al. (2002a) and the shocked albitite chips spectra presented here.

RESULTS

Thermal infrared spectra

Emissivity and hemispherical reflectance spectra of the shocked albitite chips (Fig. 1) demonstrate a variety of features that change with increasing shock pressure indicative of progressive lattice disorder and formation of glass. Major absorptions at 1150, 1037, and 1005 cm^{-1} (8.7, 9.6, and 9.9 μm) decrease in band strength with increasing pressure and coalesce into a single broad band near 1035 cm^{-1} (9.7 μm) at 55.8 GPa. Weaker absorptions that also decrease in band strength with pressure include those at 655, 600, 532, 400, and 373 cm^{-1} (15.3, 16.7, 18.8, 23.8, and 26.8 μm). The minor sharp band at 460 cm^{-1} (21.7 μm) first disappears and then develops into a broader band centered near 450 cm^{-1} (22.2 μm) in a manner
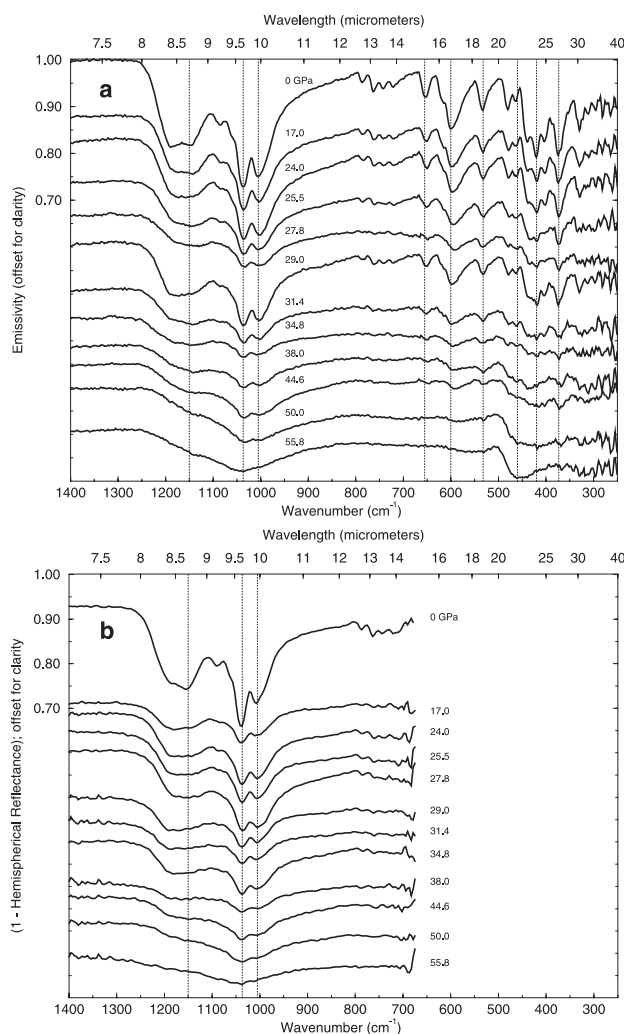

FIGURE 1. (a) Emissivity spectra of albitite chips recovered from shock experiments, with shock pressures labeled above each spectrum. **(b)** Hemispherical reflectance spectra (inverted to emissivity) of the albitite chips. Vertical dotted lines indicate spectral features that vary with increasing pressure: 1150, 1037, 1005, 655, 600, 532, 460, 420, and 373 cm^{-1} (see text). All spectra are offset from the unshocked (0 GPa) spectrum in each plot.

similar to the anorthosite spectra of Johnson et al. (2002a). Unlike the anorthosite spectra, however, no changes to the position of band centers or the Christiansen feature (the emissivity maximum near 1250 cm^{-1}) are noted for the albitite spectra.

TABLE 2. End-member library used in MESMA deconvolutions

Andesine BUR-240	Bronzite BUR-1920	Forsterite BUR-3720A
Serpentine HS-8.4B	Muscovite WAR-5474	Oligoclase WAR-0234
Biotite BUR-840	Albite WAR-0612	Actinolite HS-116.4B
Enstatite HS-9.4B	Chlorite WAR-1924	Microcline BUR-3460
Hematite BUR-2600	Quartz BUR-4120	Labradorite WAR-4524
Augite BUR-620	Gypsum var. Alabaster ML-S11	Anhydrite ML-S9
Calcite ML-C9	Dolomite C17	Augite NMNH-119197
Diopside NMNH-R17421	Fayalite WAR-RGFAY01	Hornblende NMNH-R7208
Bytownite WAR-1384	Anorthite BUR-340	Kaolinite KGa-1b solid
Ca-montmorillonite STx-1 solid	Na-montmorillonite SWy-2 solid	Nontronite WAR-5108 granular
Fe-smectite SWa-1 granular	Hedenbergite NMNH-16168	Potassium-rich_glass
Silica-rich_glass	Albitite	Anorthosite

Note: All end-members acquired from Christensen et al. (2000b), except for K and Silica glasses, which were from Wyatt et al. (2001), Hamilton et al. (2001), and the unshocked albitite (this work) and anorthosite (Johnson et al. 2002a).

Figure 2 shows emissivity and hemispherical reflectance spectra of the shocked albitite powders. Although the fine grain size of the powder subdues most of the bands observed in the spectra of the chips (e.g., Salisbury and Walter 1989), a relative reduction in band depths with increasing pressure still occurs. Volume scattering causes a transparency band at 855 cm^{-1} (11.7 μm) (e.g., Salisbury 1993). This band also decreases in strength with pressure, similar to the 830 cm^{-1} (12.0 μm) transparency band in anorthosite powders from Johnson et al. (2002a). The Christiansen feature positions of the albitite spectra are consistent with those observed for albitite powders by Nash and Salisbury (1991).

In Figure 3, band depths for five features associated with the albitite chip spectra and the band depth of the transparency feature of the powders are shown as a function of pressure for emission and reflectance spectra. Also shown are correlation lines and their associated coefficients, which range from –0.84 to –0.99. Slight differences in correlation coefficients between emission and reflectance data likely represent the minor differences in spectral resolution and acquisition techniques between the two methods. Moreover, those band depths that are least well correlated to pressure (e.g., BD_1037, BD_1005, and BD_600) are consistently those for which the band effectively disappears at pressures above about 35 GPa.

Spectral deconvolutions

Figure 4a presents the results of the spectral deconvolutions for three representative pressures (17, 27, and 56 GPa) for the albitite and anorthosite samples (Johnson et al. 2002a). End-member abundances are shown in Table 3, along with the resulting rms errors from the deconvolution runs. Uncertainties in the end-member abundances are about 5–10%. Experience has shown that end-members with abundances <5% are often selected by the algorithm to model minor residual spectral features and improve overall fits, although such minerals may not occur in the sample (cf., Christensen et al. 2000a; Hamilton et al. 2001; Bandfield 2002). Figure 4b presents spectra of the

dominant end-members selected in the deconvolution runs (i.e., those with >5% abundance) (Table 3). Figure 5 compares the rms errors for the anorthosite and albitite deconvolution results as a function of pressure.

The anorthosite shocked to 17 GPa was modeled well with a combination of unshocked anorthosite, anorthite, and bytownite. At 27 GPa, anorthite was the dominant end-member selected, although clay minerals such as serpentine and Fe-smectite were also chosen, with a corresponding increase in the rms error. At 56 GPa, anorthite and bytownite comprised 50% of the selected end-members, but were reported again in combination with 30% serpentine and Fe-smectite clays. Such clays exhibit two major absorption bands near 1050 cm^{-1} and 450 cm^{-1} (cf., Christensen et al. 2000b) that are grossly similar to the two main shocked anorthosite bands. The rms error was highest at this pressure, and the overall fit appears relatively poor (Fig. 4a). Figure 5 shows that the small rms errors at low pressures increase substantially between ~20 and 40 GPA, corresponding to the gradual onset and establishment of structural disorder in the feldspar lattice. The increase in rms errors at high shock levels implies that components in the spectral library cannot model the spectral shape of highly shocked anorthosite very well.

The 17 GPa albitite spectrum was modeled relatively well by the unshocked albitite and a bytownite feldspar, but with higher rms error than the 17 GPa anorthosite. The higher error may occur because albite exhibits a greater number of narrow spectral bands than anorthite, and the deconvolution technique is more sensitive to subtle variations in these bands between the 0 and 17 GPa albitite samples. At 27 GPa, the reported end-members included clay minerals and more calcic feldspars in place of albite, with a corresponding increase in rms error. At 56 GPa, nearly 50% clay mineral abundance was reported, although the rms error was similar to the 27 GPa fit. Indeed, the albitite rms errors are more constant with increasing pressure compared to shocked anorthosite deconvolutions (Fig. 5). This result may occur because the two main bands in the Fe-smectite
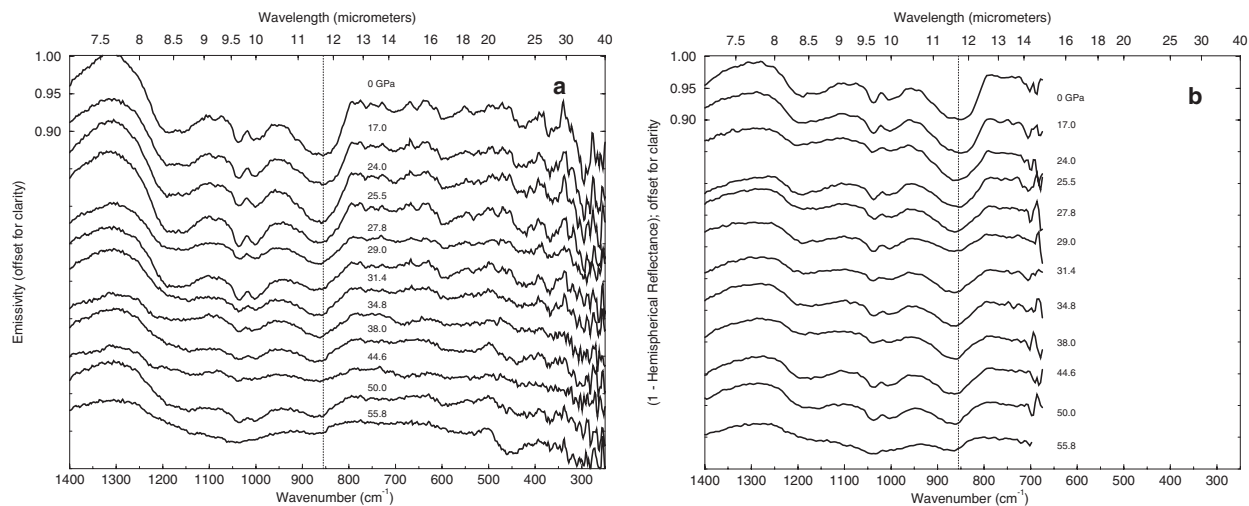

FIGURE 2. (a) Emissivity spectra of albitite powders recovered from shock experiments, with shock pressures labeled above each spectrum. **(b)** Hemispherical reflectance spectra (inverted to emissivity) of the albitite powders. All spectra are offset from the unshocked (0 GPa) spectrum. Vertical dotted line at 855 cm^{-1} locates a transparency feature that varies with increasing pressure as described in text.
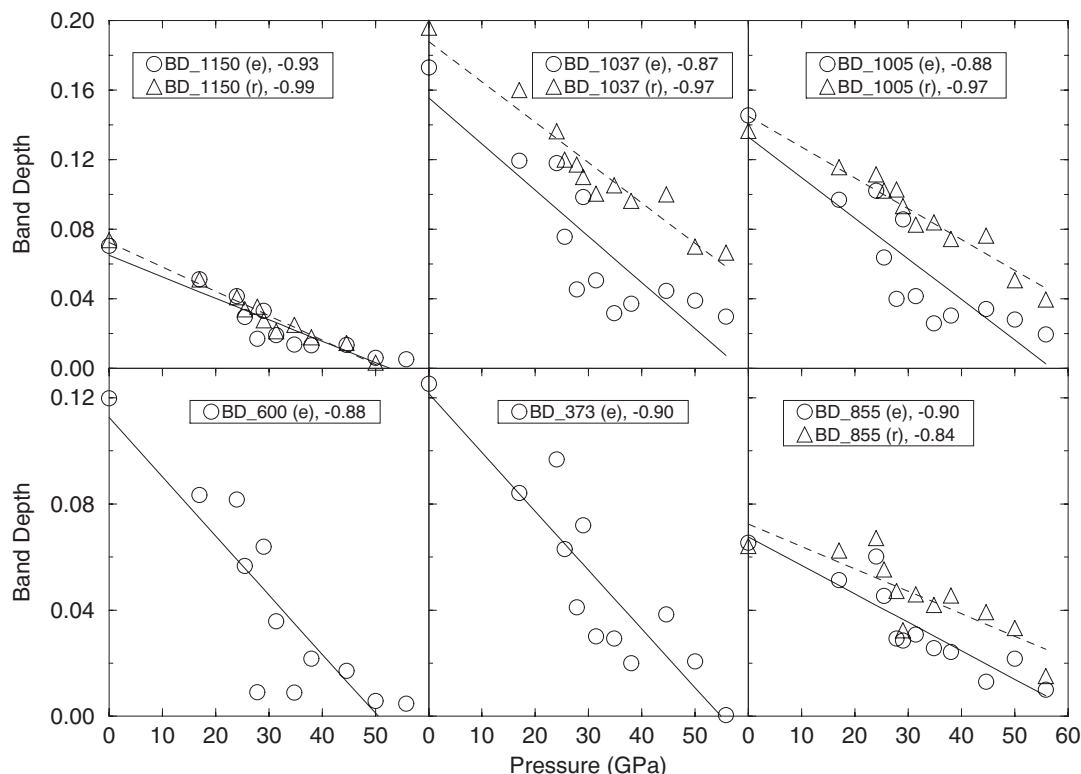
FIGURE 3. Decrease in band depths (BD) of six bands as a function of shock pressure for emissivity (e) and (where available) hemispherical reflectance (r) spectra of albitite. Band depths computed using continuum between the following wavenumbers: BD_1150 (1110 cm^{-1} and 1210 cm^{-1}); BD_1037, BD_1005 (960 cm^{-1} and 1110 cm^{-1}); BD_855 (794 cm^{-1} and 951 cm^{-1}); BD_600 (500 cm^{-1} and 635 cm^{-1}); and BD_373 (345 cm^{-1} and 500 cm^{-1}). All band depths are from spectra of chips except for BD_855, which is from the powders. Correlation lines shown (solid for emissivity; dashed for reflectance), with correlation coefficients listed in legend.

and serpentine clays described above are more similar to the two main bands in highly shocked albitite than the similarly shocked anorthosite (Fig. 4b).

DISCUSSION

In shocked samples, crystalline and amorphous phases are likely to coexist as intimate mixtures with the proportion of diaplectic glass increasing with shock pressure (Ostertag 1983; Heymann and Hörz 1990; Yamaguchi and Sekine 2000), resulting in the gradual disappearance of absorption bands in thermal infrared spectra. For example, small bands between 500 and 650 cm^{-1} fade away by about 45 GPa because of depolymerization of the silica tetrahedra (e.g., Williams 1998). This behavior is similar to that observed in absorption spectra of shocked Na-rich feldspars by Ostertag (1983), as is the appearance of the band near 460 cm^{-1} with increasing pressure (Fig. 1). The stronger Si-O stretching bands at higher wavenumbers (1150, 1037, and 1005 cm^{-1}) disappear by about 50 GPa.

The 855 cm^{-1} transparency feature in powdered albitite samples (Fig. 2) is caused by their fine grain size, which reduces the spectral contrast of the reststrahlen bands and allows volume scattering to dominate (e.g., Salisbury et al. 1991a, 1991b). The transparency feature disappears almost completely at the highest pressures, likely because the structural disorder

TABLE 3. Deconvolution results for selected albitite and anorthosite spectra

| Pressure	Albitite		RMS error	Anorthosite		RMS error
17 GPa	Albitite	61%	0.0053	Anorthosite	47%	0.0022
	Bytownite	26%		Anorthite	26%	
	Andesine	4%		Bytownite	18%	
	Labradorite	3%		Diopside	3%	
	Dolomite	2%		Fayalite	2%	
	Calcite	2%		Dolomite	2%	
	Microcline	2%		K glass	1%	
	Fayalite	<1%		Muscovite	1%	
	Chlorite	<1%		Gypsum	<1%	
27 GPa	Bytownite	35%	0.0069	Anorthite	48%	0.0089
	Fe-smectite	26%		Serpentine	17%	
	Albitite	15%		Fayalite	9%	
	Andesine	12%		Dolomite	7%	
	Serpentine	7%		Fe-smectite	6%	
	Dolomite	3%		Nontronite	4%	
	Hematite	<1%		Hornblende	4%	
	Chlorite	<1%		Bytownite	3%	
	Microcline	<1%		Forsterite	2%	
56 GPa	Fe-smectite	26%	0.0065	Anorthite	37%	0.0097
	Bytownite	18%		Serpentine	17%	
	Serpentine	16%		Fe-smectite	13%	
	Anorthite	14%		Bytownite	13%	
	K glass	11%		Fayalite	10%	
	Microcline	7%		Dolomite	6%	
	Ca-mont.	6%		K glass	3%	
	Dolomite	3%		Forsterite	<1%	
	Kaolinite	<1%				
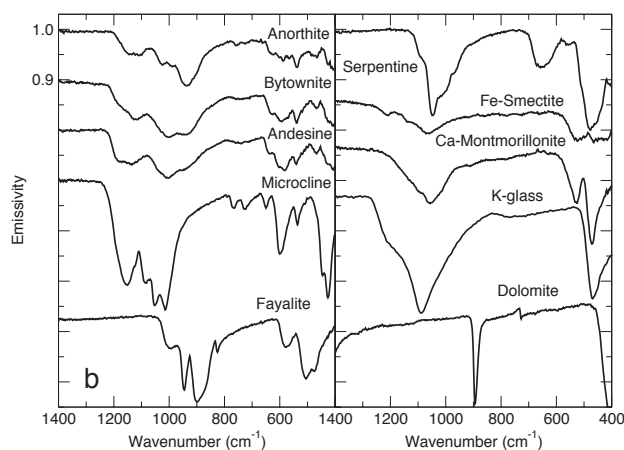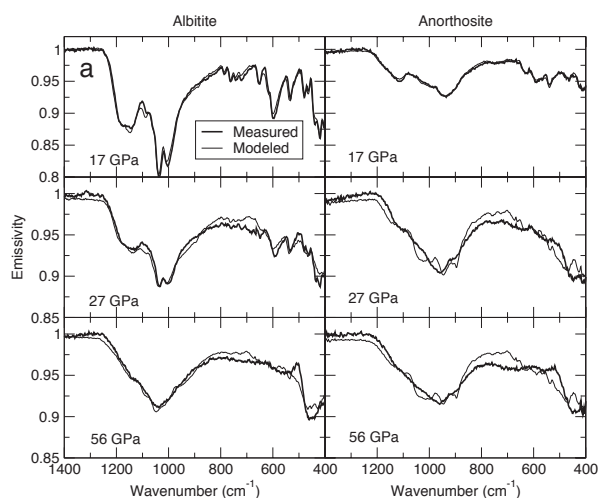
FIGURE 4. (a) Comparison of measured (thick line) and deconvolved (modeled; thin line) spectra of albitite (left) and anorthosite (right) chips of shocked samples (17 GPa, 27 GPa, and 56 GPa) (cf., Johnson et al. 2002a). **(b)** Spectra of end-members selected from deconvolutions at abundances >5% (Table 3).
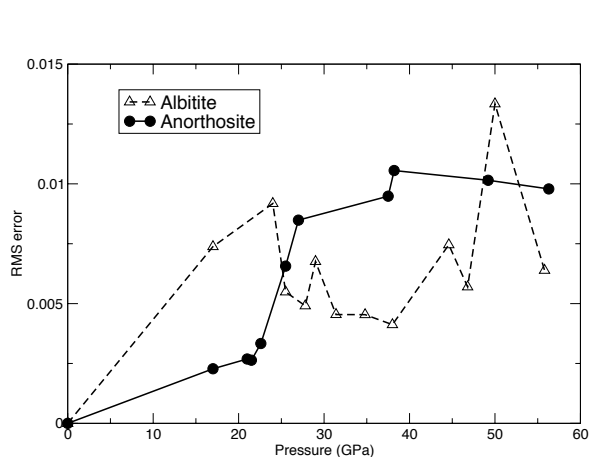

FIGURE 5. Comparison of rms error values from spectral deconvolution runs between albitite and anorthosite. Increase in anorthosite rms values near 20 GPa suggests that no spectral library end-members are available to model the change in spectral shape due to the onset of diaplectic glass formation. Conversely, the albitite sample has higher rms values that change relatively little with increasing pressure.
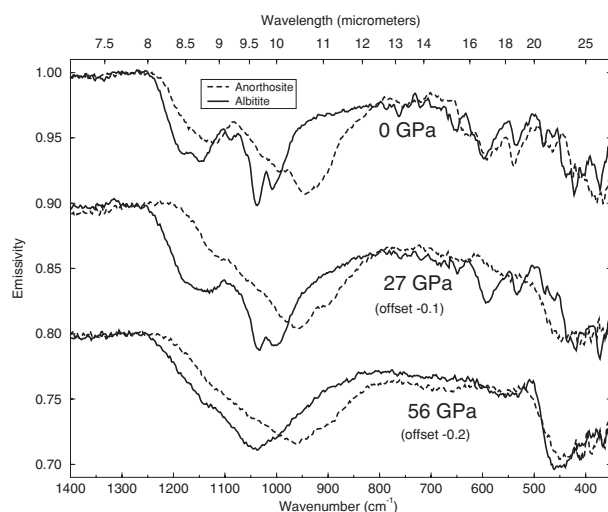

FIGURE 6. Comparison of anorthosite and albitite spectra of unshocked (0 GPa) and shocked samples (27 GPa, 56 GPa; with offsets as shown; cf., Johnson et al. 2002a). For plotting purposes, the spectral contrast of the unshocked albitite sample was decreased to match that of anorthosite. Note persistence of spectral features in albitite sample at 27 GPa relative to the anorthosite sample.

at these pressures prevents significant volume scattering. Nash and Salisbury (1991) observed a similar effect in their spectra of fused albite glass.

Figure 6 compares three spectra of albitite and anorthosite to demonstrate how the spectral features in albitite are maintained to higher pressures than similar features in anorthosite. For example, the bands near 535 and 600 cm^{-1} (Si-O-Si bending vibrations) are still apparent at 27 GPa in the albitite spectrum but not in the anorthosite. Similarly, the Si-O antisymmetric stretching band at 1115 cm^{-1} in anorthosite is nearly gone at this pressure whereas the 1150 cm^{-1} band in the albitite is maintained. At the highest pressures, both types of

feldspars have lost all but two major features, the deep band near 440–460 cm^{-1} (caused by bending vibrations in the Si-O-Al planar ring structures) and the broad Si-O stretch bands at 960 cm^{-1} (anorthosite) and 1035 cm^{-1} (albitite).

The persistence of the albitite bands to higher pressures than the anorthosite is consistent with previous thermal infrared absorption and Raman spectroscopic studies (e.g., Ostertag 1983; Velde et al. 1989; Heymann and Hörz 1990; Williams 1998). This difference is depicted further in Figure 7, in which the band areas between 505 and 555 cm^{-1} are calculated from the anorthosite and albitite spectra. The anorthosite band areas approach zero around 27–29 GPa (negative band areas are
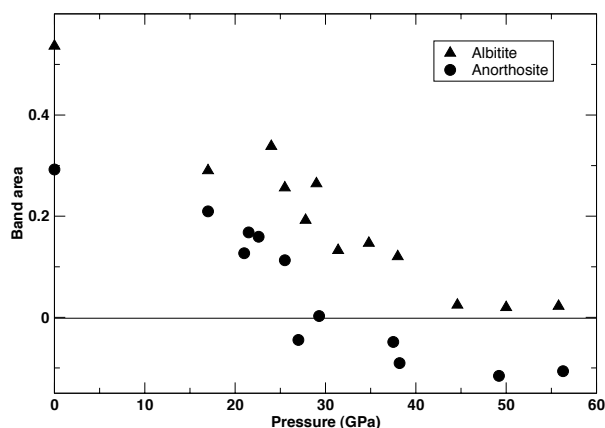
FIGURE 7. Band areas calculated between 505 and 555 cm^{-1} for anorthosite and albitite spectra, demonstrating the greater persistence of the albitite band at higher shock pressures compared to the anorthosite band. Negative band areas in the anorthosite are caused by the shoulder of the 450 cm^{-1} band.

caused by the shoulder of the 450 cm^{-1} band), whereas the albitite band areas do not approach zero until about 40–45 GPa. This difference in feldspar response to high pressures may result from the higher Al content in anorthite relative to albite. Previous work has suggested that the coordination changes of tetrahedral cations appear to occur at lower pressures for AlO$_4$ tetrahedra than for SiO$_4$ tetrahedra (Williams 1998).

Spectral deconvolutions of the data presented here are valuable to determine the uniqueness of the shocked feldspar spectra relative to combinations of common minerals, which is particularly relevant to deconvolutions of remotely sensed spectra. The results shown above suggest that, although anorthosite spectra at low to intermediate shock pressures may be modeled relatively well by the dominant feldspar (plus some nearby solid-solution members and some minor minerals), once the shock pressures reach 25–30 GPa the ability to model the shocked spectra accurately decreases sharply. Conversely, deconvolutions of the albitite spectra have no apparent correlation with pressure, perhaps owing to the greater similarity of the two major clay mineral absorption features to those in more highly shocked albitites (Fig. 4b). Without this similarity, albitite probably would show the same trend of increasing rms error with pressure as does anorthosite. But because of this similarity, it is possible that deconvolutions could select these types of clay minerals in place of highly shocked albite (or vice-versa).

Implications for remote sensing

Thermal infrared emission and reflectance spectroscopy of experimentally shocked plagioclase feldspars demonstrate how the increase in structural disorder induced by high pressures is manifested in a degradation of their spectral absorptions. Characteristic absorptions related to the bending and stretching motions of Si and Al tetrahedra in the thermal infrared are lost with increasing pressure, with spectral features in albite-rich feldspars persisting to higher pressures than similar absorption bands in anorthite-rich feldspars, possibly owing to the higher

Al content in anorthite. Further work on intermediate composition plagioclase feldspars could be useful in constraining this resilience to high shock pressures.

Spectra of highly shocked anorthosites are represented more poorly by linear mixtures of common minerals than are mildly shocked samples. Conversely, model errors of shocked albitite spectra show little correlation with pressure. The unique nature of highly shocked anorthosite spectra suggests that they are more appropriate to use in deconvolutions of remotely sensed spectra than are shocked albitite spectra. However, albite is not a common mineral on planetary surfaces other than on Earth. Indeed, the feldspar compositions detected on Mars by the Thermal Emission Spectrometer (TES) have been dominantly intermediate to calcic plagioclase (e.g., Christensen et al. 2001; Bandfield 2002). Johnson et al. (2002b) performed preliminary deconvolutions of TES spectra of impact crater regions on Mars using shocked anorthosite spectra in spectral end-member libraries to identify areas of highly shocked materials. Further TES data analysis is ongoing and will be combined with spectra from additional shock experiments using basaltic rocks and data from the Thermal Multispectral Imaging System currently in orbit on the Mars Odyssey spacecraft (Christensen et al. 1999) and the Mini-TES instrument carried by the Mars Exploration Rovers (Squyres et al. 2001).

REFERENCES CITED

Arndt, J., Hummel, W., and Gonzalez-Cabeza, I. (1982) Diaplectic Labradorite glass from the Manicouagan impact crater, I. Physical properties, crystallization, structural and genetic implications. Physics and Chemistry of Minerals, 8, 230–239.

Bandfield, J.L. (2002) Global mineral distributions on Mars. Journal of Geophysical Research, 107 (E6), 10.1029/2001JE001510.

Bunch, T.E., Cohen, A.J., and Dence, M.R. (1967) Natural terrestrial maskelynite. American Mineralogist, 52, 244–253.

———(1968) Shock-induced structural disorder in plagioclase and quartz, in Shock Metamorphism of Natural Materials, Proceedings of the First Conference, Mono Book Corp., Baltimore, 509–518.

Christensen, P.R. and 11 others (1998) Results from the Mars Global Surveyor Thermal Emission Spectrometer. Science, 279, 1692–1698.

Christensen, P.R., Jakosky, B.M., Kieffer, H.H., Malin, M.C., McSween, Jr., H.Y., K. Nealson, K., Mehall, G., Silverman, S., and Ferry, S. (1999) The thermal emission imaging system (THEMIS) instrument for the Mars 2001 orbiter. Lunar and Planetary Science Conference XXX, Abstract 1470.

Christensen, P.R. and 15 others (2000a) Detection of crystalline hematite mineralization on Mars by the Thermal Emission Spectrometer: Evidence for near-surface water. Journal of Geophysical Research, 105, 9623–9642.

Christensen, P.R., Bandfield, J.L., Hamilton, V.E., Howard, D.A., Lane, M.D., Piatek, J.L., Ruff, S.W., and Stevanov, W.L. (2000b) A thermal emission spectral library of rock-forming minerals. Journal of Geophysical Research, 105, 9735–9739.

Christensen, P.R. and 25 others (2001) The Mars Global Surveyor thermal emission spectrometer experiment: Investigation description and surface science results. Journal of Geophysical Research, Journal of Geophysical Research, 106, 23,823–23,871.

Cooney, T.F., Scott, E.R.D., Krot, A.N., Sharma, S.K., and Yamaguchi, A. (1999) Vibrational spectroscopic study of minerals in the Martian meteorite ALH84001. American Mineralogist, 84, 1569–1576.

Daniel, I., Gillet, P., and Ghose, S. (1995) A new high-pressure phase transition in anorthite (CaAl$_2$Si$_2$O$_8$) revealed by Raman spectroscopy. American Mineralogist, 80, 645–648.

Daniel, I., Gillet, P., McMillan, P.F., Wolf, G., and Verhelst, M.A. (1997) High-pressure behavior of anorthite: Compression and amorphization. Journal of

Geophysical Research, 102, 10,313–10,325.
DeCarli, P.S., Bowden, E., Jones, A.P., and Price, G.D. (2002) Laboratory impact experiments versus natural impact events. In Koeberl, C., and MacLeod, K.G., Eds., Catastrophic Events and Mass Extinctions: Impacts and Beyond, 356, 595–605.Geological Society of America Special Paper, Boulder, Colorado.
Delaney, J.S., Dyar, M.D., Hörz, F., and Johnson, J.R. (2003) Evidence for coordination and redox changes of iron in shocked feldspar from synchrotron microXANES. Lunar and Planetary Science Conference XXXIV, abstract 1417.
Fritz, J., A. Greshake, A., Hecht, L., and Stöffler, D. (2002) Shock metamorphism of Martain meteorites: New data from quantitative shock barometry. Lunar and Planetary Science Conference XXXIII, Abstract 1504.
Gibbons, R.V., Morris, R.V. Hörz, F., and Thompson, T.D. (1975) Petrographic and ferromagnetic resonance studies of experimentally shocked regolith analogs. Proceedings of the Lunar Science Conference 6th, 3143–3171.
Hamilton, V.E., Wyatt, M.B., McSween, Jr., H.Y., and Christensen, P.R. (2001) Analysis of terrestrial and martian volcanic compositions using thermal emission spectroscopy: II. Application to martian surface spectra from the Mars Global Surveyor Thermal Emission Spectrometer. Journal of Geophysical Research, 106, 14,733–14,746.
Heymann, D. and Hörz, F. (1990) Raman-spectroscopy and X-ray diffractometer studies of experimentally produced diaplectic feldspar glass. Physics and Chemistry of Minerals, 17, 38–44.
Hörz, F. and Cintala, M. (1997) Impact experiments related to the evolution of planetary regoliths. Meteoritics and Planetary Science, 32, 179–209.
Iiishi, K., Tomisaka, T. Kato, T., and Umegaki, Y. (1971) Isomorphous substitution and infrared and far infrared spectra of the feldspar group. Neues Jahrbuch für Mineralogie. Abhandlungen, 115, 98–119.
Johnson, J.R., Lucey, P.G., Horton, K.A., and Winter, E.M. (1998) Infrared measurements of pristine and disturbed soils 1. Spectral contrast differences between field and laboratory data. Remote Sensing of Environment, 64, 34–46.
Johnson, J.R., Hörz, F., Christensen, P., and Lucey, P.G. (2002a) Thermal infrared spectroscopy of experimentally shocked anorthosite and pyroxenite: Implications for remote sensing of Mars. Journal of Geophysical Research, 107(E10), 10.1029/2001JE001517.
Johnson, J.R., Staid, M.I., and Titus, T.N. (2002b) Shocked plagioclase signatures in Thermal Emission Spectrometer data of Mars. Lunar and Planetary Science Conference XXXIII, Abstract 1345.
Jones, A.H., Isbell, W.M., and Maiden, J.C. (1966) Measurements of the very-high-pressure properties of materials using a light-gas gun. Journal of Applied Physics, 37, 3493–3499.
Lyon, R.J.P. (1963) Evaluation of infrared spectrophotometry for compositional analysis of lunar and planetary soils. NASA Technical Note D-1871.
Marsh, S.P. (1980) LASL Shock Hugoniot Data. University of California Press, Berkeley, 658 pp.
Morris, P.W., Heras, A.M., Vandenbussche, B., and Dijkstra, R. (1999) Asteriod 4 Vesta as seen with the infrared space observatory short wavelength spectrometer. LPI Contribution, Report 969, 19–20.
Mustard, J.F. and Hays, J.E. (1997) Effects of hyperfine-particles on reflectance spectra from 0.3 to 25 μm. Icarus, 125, 145–163.
Muszynski, M. and Natkaniec-Nowak, L. (1992) Albites and oligoclasite from Szklary (Lower Silesia). Bulletin of the Polish Academy of Science and Earth Science, 40, 141–159.
Nash, D.B. and Salisbury, J.W. (1991) Infrared reflectance spectra (2.2–15 μm) of plagioclase feldspars. Geophysical Research Letters, 18, 1151–1154.
Ostertag, R. (1983) Shock experiments on feldspar crystals. Proceedings of the 14th Lunar and Planetary Science Conference. Journal of Geophysical Research, 88, B364–B376.
Ramsey, M.S. (2002) Ejecta distribution patterns at Meteor Crater, Arizona: On the applicability of lithologic endmember deconvolution for spaceborne thermal infrared data of Earth and Mars. Journal of Geophysical Research, 107(E8), 10.1029/2001JE001827.
Roberts, D.A., Gardner, M., Church, R., Ustin, S., Sheer, G., and Green, R.O. (1998). Mapping Chaparral in the Santa Monic,a mountains using multiple endmember spectral mixture models. Remote Sensing of Environment, 65, 267–269.
Ruff, S.W., Christensen, P.R. Barbera, P.W., and Anderson, D.L. (1997) Quantitative thermal emission spectroscopy of minerals: A technique for measurement and collection. Journal of Geophysical Research, 102, 14899–14913.
Salisbury, J.W. (1993) Mid-infrared spectroscopy: Laboratory data. In C. Pieters and P. Englert, Eds., Remote Geochemical Analysis, Chapter 4. Cambridge University Press, New York.
Salisbury, J.W. and Walter, L.S. (1989) Thermal infrared (2.5–13.5 μm) spectroscopic remote sensing of igneous rock types on particulate planetary surfaces. Journal of Geophysical Research, 94, 9192–9202.

Salisbury, J.W., D'Aria, D.M., and Jarosewich, E. (1991a) Midinfrared (2.5–13.5 μm) reflectance spectra of powdered stony meteorites. Icarus, 92, 280–297.
Salisbury, J.W., Walter, L.S., Vergo, N., and D'Aria, D.M. (1991b) Infrared (2.1–25 μm) Spectra of Minerals. The Johns Hopkins University Press, Baltimore, 267 pp.
Salisbury, J.W., Wald, A., and D'Aria, D.M. (1994) Thermal-infrared remote sensing and Kirchhoff's law 1. Laboratory measurements. Journal of Geophysical Research, 99, 11897–11911.
Salisbury, J.W., Murcray, D.G., Williams, W.J., and Blatherwick, R.D. (1995) Thermal infrared spectra of the Moon. Icarus, 115, 181–190.
Salisbury, J.W., Basu, A., and Fischer, E.M. (1997) Thermal infrared spectra of lunar soils. Icarus, 130, 125–139.
Sprague, A.L., Emery, J.P., Donaldson, K.L., Russell, R.W., Lynch, D.K., and Mazuk, A.L (2002) Mercury: Mid-infrared (3–13.5 μm) observations show heterogeneous composition, presence of intermediate and basic soil types, and pyroxene. Meteoritics and Planetary Science, 37, 1255–1268.
Staid, M. I., Gaddis, L.R., and Titus, T. (2001) A new approach for mapping minerals on Mars with TES data. EOS, Transactions of the American Geophysical Union (abstract), P42A–0553.
Stöffler, D. (1971) Progressive metamorphism and classification of shocked and brecciated crystalline rocks at impact craters. Journal of Geophysical Research, 76, 5541–5551.
———(1972) Deformation and transformation of rock-forming mineral by natural and experimental shock processes I. Behavior of minerals under shock compression. Fortschrift für Mineralogie, 49, 50–113.
———(1974) Deformation and transformation of rock-forming minerals by natural and experimental shock processes, II. Physical properties of shocked minerals. Fortschrift für Mineralogie, 51, 256–289.
———(1984) Glasses formed by hypervelocity impact, Journal of Non-Crystalline Solids, 67, 465–502.
———(2001) Maskelynite confirmed as diaplectic glass: Indication for peak shock pressures below 45 GPa in all Martian meteorites. Lunar and Planetary Science Conference XXXII, Abstract 1170.
Stöffler, D. and Hornemann, U. (1972) Quartz and feldspar glasses produced by natural and experimental shock. Meteoritics, 7, 371–394.
Squyres, S.W., Arvidson, R.E., Bell III, J.F. Carr, M., Christensen, P., DesMarais, D., Economous, T., Gorevan, S., Haskin, L., and Herkenhoff, K. (2001) The Athena science payload for the 2003 Mars Exploration Rovers. First Landing Site Workshop for the 2003 Mars Exploration Rovers, p. 65.
Thomson, J. and Salisbury, J. (1993) The mid-infrared reflectance of mineral mixtures (7–14 μm). Remote Sensing of Environment, 45, 1–13.
Therkelsen, J.P. (2002) Shock induced changes in redox state of experimentally shocked plagioclase, pyroxenite, and olivine. B.A. Thesis, Amherst College, 98 p.
Velde, B., Syono, Y., Couty, R., and Kikuchi, M. (1987) High pressure infrared spectra of diaplectic anorthite glass. Physics and Chemistry of Minerals, 14, 345–349.
Velde, B., Syono, Y., Kikuchi, M., and Boyer, H. (1989) Raman microprobe study of synthetic diaplectic plagioclase feldspars. Physics and Chemistry of Minerals, 16, 436–441.
Williams, Q. (1998) High-pressure infrared spectra of feldspars: Constraints on compressional behavior, amorphization, and diaplectic glass formation. In M.H. Manghnani and T. Yagi, Eds., Properties of Earth and Planetary Material at High Pressure and Temperature, 531–543. Geophysical Monograph 101, American Geophysical Union, Washington, D.C.
Williams, Q. and Jeanloz, R. (1988) Spectroscopic evidence for pressure-induced coordination changes in silicate glasses and melts. Science, 239, 902–905.
———(1989) Static amorphization of anorthite at 300K and comparison with diaplectic glass. Nature, 338, 413–415.
Wyatt, M.B., Hamilton, V.E., McSween, H.Y. Jr., Christensen, P.R., and Taylor, L.A. (2001) Analysis of terrestrial and martian volcanic compositions using thermal emission spectroscopy: I. Determination of mineralogy, chemistry, and classification strategies. Journal of Geophysical Research, 106, 14,711–14,732.
Xie, X., Chen, M., Dai, C, El Goresy, A., and Gillet, P. (2001) A comparative study of naturally and experimentally shocked chondrites. Earth Planetary Science Letters, 187, 345–356.
Yamaguchi, A. and Sekine, T. (2000) Monomineralic mobilization of plagioclase by shock: an experimental study. Earth Planetary Science Letters, 175, 289–296.